# Paleohydraulics of the last outburst flood from glacial Lake Agassiz and the 8200 BP cold event

Garry K.C. Clarke[a],*, David W. Leverington[b], James T. Teller[c], Arthur S. Dyke[d]

[a] Earth and Ocean Sciences, University of British Columbia, 6339 Stores Road, 219 Main Mall, Vancouver, BC, Canada V6T 1Z4
[b] Center for Earth and Planetary Studies, National Air and Space Museum, Smithsonian Institution, Washington, DC 20560-0315, USA
[c] Department of Geological Sciences, University of Manitoba, Winnipeg, Manitoba, Canada R3T 2N2
[d] Terrain Sciences Division, Geological Survey of Canada, 601 Booth Street, Ottawa, ON, Canada K1A 0E8

## Abstract

During the last deglaciation of North America, huge proglacial lakes formed along the southern margin of the Laurentide Ice Sheet. The largest of these was glacial Lake Agassiz, which formed about 11.7 ^{14}C kyr and drained into Hudson Bay about 7.7 ^{14}C kyr (8.45 cal kyr). Overflow from these lakes was variably directed to the Mississippi, St. Lawrence and Mackenzie drainage systems and it is thought that switches in routing were accompanied by a response in ocean circulation that produced abrupt climate events. When the ice dam across Hudson Bay finally was breached, a massive flood drained Lake Agassiz, which was routed through Hudson Strait to the Labrador Sea. In terms of stored water volume the largest reservoir was associated with the Kinojévis level of Lake Agassiz. For this maximum filling, the impounded water volume available to produce floods is estimated as 40,000–151,000 km$^3$, depending on the location of the ice margin and route used. The timing of this rapid release of stored freshwater just precedes the early Holocene cooling event at 8.2 cal kyr BP. We use the Spring–Hutter theory to simulate flood hydrographs for floods that originate in subglacial drainage conduits and find that flood magnitude and duration are $\sim 5$ Sv and $\sim 0.5$ yr. Multiple fillings and floods are possible as are single floods having a complex multipulse structure. Modelling results suggest that the outburst flood from Lake Agassiz may have terminated before the lake surface elevation dropped to sea level and that the flood ended when a stable drainage channel was established, connecting Lake Agassiz to the Tyrrell Sea.

## 1. Introduction

The records from the GRIP and GISP ice cores in Greenland indicate that a cold event occurred around 8.2 cal kyr BP, and was the most significant climate excursion of the past 10,000 years. At Summit this climate signal is expressed as a $\sim 5°C$ drop in mean temperature, coinciding with decreases in precipitation and atmospheric methane concentration, and increases in forest–fire frequency and dust deposition sustained over roughly 200 years (Alley et al., 1997). Changes in methane concentration, fire frequency and dust deposition imply that the 8.2 cal kyr BP event was hemispheric in character, an inference that is reinforced by a variety of terrestrial and aquatic proxies at widespread sites in the Northern Hemisphere (e.g. Hughen et al., 1996; Klitgaard-Kristensen et al., 1998; von Grafenstein et al., 1998; Baldini et al., 2002; Hass, 2002). A causal

relationship between the early Holocene drainage of ice-dammed Lake Agassiz and the 8.2 cal kyr BP cooling event had been suspected (von Grafenstein et al., 1998) but the relative timing of lake drainage and of climate deterioration seemed incompatible with this interpretation. The contribution of Barber et al. (1999) removed this impasse by establishing that the ^{14}C dates, upon which the drainage chronology for Lake Agassiz was based, were systematically biased and required an additional correction for marine reservoir effects. The approximate volume of the final lake phase had been estimated by Veillette (1994) as $114 \times 10^3$ km$^3$. It is now widely accepted that the 8.2 cal kyr BP cold event was correlative with and probably triggered by the rapid northward drainage of the superlake formed by the coalescence of glacial Lakes Agassiz and Ojibway (Teller et al., 2002). For convenience, we will refer to the coalesced superlake as Lake Agassiz rather than by the more explicit but less euphonious "glacial Lake Agassiz–Ojibway".

Although the contribution of Barber et al. (1999) solves the problem of timing, new questions present

---

*Corresponding author. Tel.: +1-604-822-3602; fax: +1-604-822-6088.

E-mail address: clarke@eos.ubc.ca (G.K.C. Clarke).

themselves: (1) How did lake drainage lead to a climate signal (Renssen et al., 2001, 2002)? (2) How much water was released (Leverington et al., 2002a)? (3) What were the magnitude and duration of the flood? (4) Was there a single northward-routed flood or several (Leverington et al., 2002a; Teller et al., 2002)? (5) What is the implication of the two-pronged character of the 8.2 cal kyr BP climate signal as it appears in the Greenland accumulation record (Alley et al., 1997), speleothems in Ireland (Baldini et al., 2002) and the sedimentary record of European lakes (e.g. von Grafenstein et al., 1998)? The present contribution focuses on questions (3)–(5).

## 2. Lake Agassiz outbursts and the geomorphic record

Proglacial Lake Agassiz was established around 11.7 $^{14}$C kyr as the southern margin of the Laurentide Ice Sheet (LIS) retreated northward; the lake may have persisted until around 7.5 $^{14}$C kyr when its level dropped to that of the Tyrrell Sea (Teller, 1987). Rapid changes in the configuration of the LIS, isostatic adjustments for the changing load of ice and water, and the topography of the newly deglaciated surface resulted in complex overflow and bathymetric histories (e.g. Teller, 1987, 2003; Licciardi et al., 1999; Leverington et al., 2000, 2002a). At various times during its 5000 yr (4000 radiocarbon year) existence, overflow from Lake Agassiz was routed to the Mississippi–Great Lakes–St. Lawrence and Mackenzie drainage systems (Teller, 1990a, b; Licciardi et al., 1999; Teller et al., 2002) but only in the final stages was the barrier of the LIS breached and Lake Agassiz water routed northward to Hudson Bay. Key papers relating to Lake Agassiz and the ice-marginal fringe of proglacial lakes include those by Upham (1895), Johnston (1946), Elson (1967), Hardy (1977), Vincent and Hardy (1977, 1979), Dredge (1983), Klassen (1983), Teller and Thorleifson (1983), Veillette (1994), Mann et al. (1999), Marshall and Clarke (1999), Clark et al. (2001) and Teller (2001).
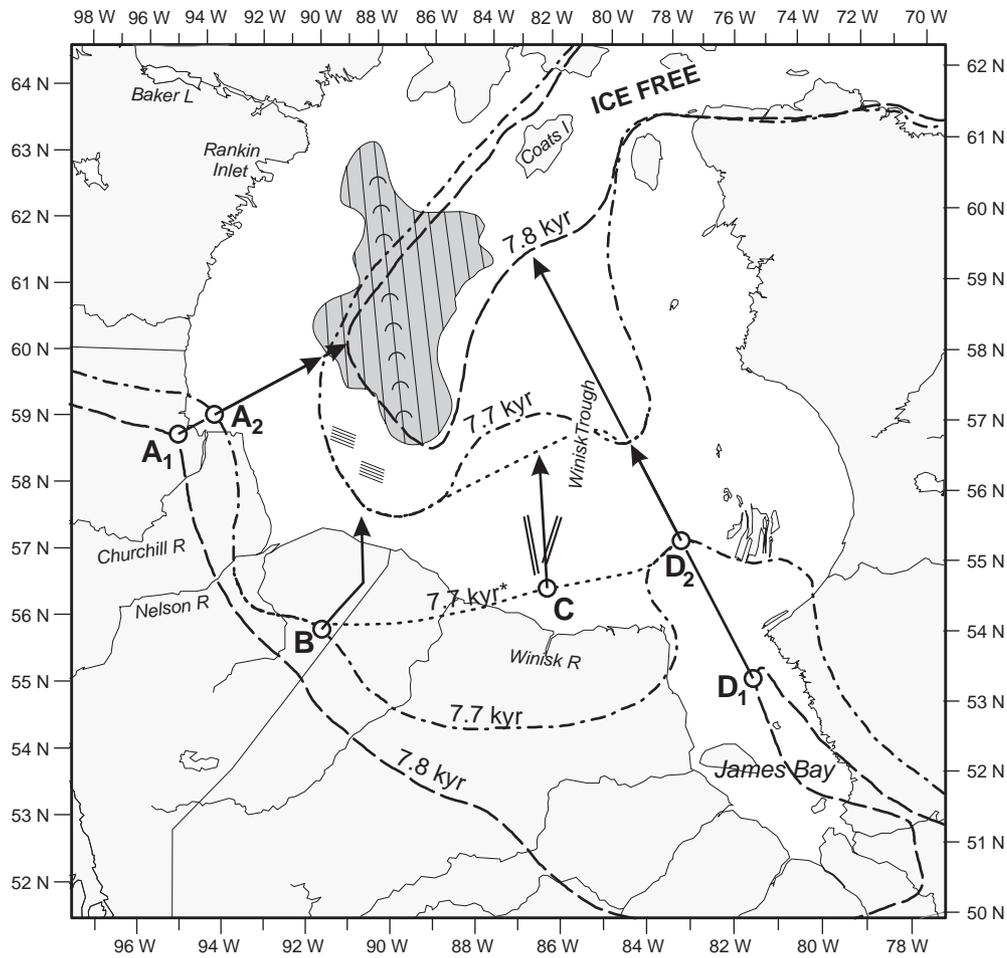
Given the northward-sloping land surface and a disintegrating ice barrier, formed by the LIS, final northward routing of Agassiz water would have been inevitable. Following the last (Cochrane) surges of the LIS into the Hudson Bay Lowlands (e.g. Hardy, 1977; Dredge and Cowan, 1989; Vincent, 1989) and across Hudson Strait (e.g. Andrews et al., 1995; Kerwin, 1996; Jennings et al., 1998) about 8300–8000 $^{14}$C yr BP, there was a collapse of ice over Hudson Bay, and marine waters invaded the northeastern part of the Hudson Bay basin from Hudson Strait. This incursion and the subsequent outburst from Lake Agassiz–Ojibway are recorded by the nature, fauna and provenance of dated sediments in Hudson Strait (e.g. Andrews et al., 1995; Kerwin, 1996); the details of the outburst are summarized in Barber et al.

(1999), who revised radiocarbon ages of carbonate in Hudson Strait and Hudson Bay by 85–310 yr, and concluded that proglacial Lakes Agassiz and Ojibway drained about 7.7 $^{14}$C kyr BP (8.45 cal kyr BP). Ice along the southern margin of the LIS retreated after the Cochrane surges, as proglacial lakes expanded northward; evidence from the southern side of the LIS for the timing of the final drainage of the coalesced Lake Agassiz–Ojibway has been presented by Hardy (1977), Vincent and Hardy (1979), Veillette (1994), Dredge and Cowan (1989), Vincent (1989) and others.

Geomorphic evidence for a glacier outburst flood into Hudson Bay is not abundant, possibly because much of the region through which floods would be routed was below sea level. Evidence for one or more northward outbursts from Lake Agassiz comes from surface mapping (e.g. Dredge, 1983; Klassen, 1983) and from a marine geophysical survey of Hudson Bay (Josenhans and Zevenhuizen, 1990) which yielded classical as well as exotic evidence for intense floods (Fig. 1). The location of drainage routes A$_1$, A$_2$, B and C in Fig. 1 are largely based on this geomorphic evidence on the floor of Hudson Bay; routes along D are based on interpretations by Vincent and Hardy (1979) and Veillette (1994). Classical evidence includes the presence of kilometre-wide meltwater channels eroded through glacial diamict to bedrock and considered by Josenhans and Zevenhuizen (1990) to be of late glacial age. The presence of megaripple sand-wave bed forms provides probable evidence for large discharge in offshore Hudson Bay. It is difficult to dismiss this evidence by attributing these features to normal subglacial water flow because if the surface slope of the ice sheet over Hudson Bay was very low at the late stages of deglaciation, as would be expected for a downwasting ice mass, then the topographic drive for water flow was also small. High-energy geomorphic features could only be produced if the discharge rate was very high. Thus late-forming high-energy features such as the meltwater channels and sand waves are likely to have been formed by floods from the lake. Exotic evidence for flooding is provided by an areally extensive region of arcuate iceberg scours on the floor of Hudson Bay (Fig. 1). The most plausible explanation for these unusual features is that grounded multi-keeled tabular icebergs were mobilized by fast-flowing water and, in turn, one keel served as a pivot point while others inscribed arcs on the sea floor (Josenhans and Zevenhuizen, 1990; Dyke, 2003). The arcuate scours tend to be convex in the same direction, implying unidirectional current flow.

## 3. Flood physics

During the final phases of Lake Agassiz, its level was maintained by a spillway to the St. Lawrence drainage

Fig. 1. Ice margins, prospective drainage routings and geomorphic constraints for outburst floods from glacial Lake Agassiz. Ice margins for 7.8 ^{14}C kyr BP (long-dashed line) and 7.7 ^{14}C kyr BP (dot-dashed lines) are from Dyke (2003). An adjusted ice margin labelled 7.7 kyr* (short-dashed lines) is also proposed to acknowledge mapped meltwater channels. Submarine geomorphic features consistent with outburst floods from Lake Agassiz include sandwaves, arcuate iceberg scours, meltwater channels incised into glacial deposits and the Winisk Trough feature (Josenhans and Zevenhuizen, 1990).

system (e.g. Vincent and Hardy, 1979; Leverington et al., 2002a) while simultaneously the ice dam was thinning and decreasing in width as both the northern margin of the LIS retreated southward and the southern margin retreated northward (Fig. 1; Dyke and Prest, 1987). In terms of a release mechanism, the most important consideration is the obvious one that ice floats on water so that, typically, subglacial outburst floods have precedence over supraglacial floods. Although the LIS ice dam may have physically failed, we consider this an unlikely possibility because the dam was probably very wide relative to its thickness and would not therefore have been susceptible to mechanical failure. We believe the final drainage of Lake Agassiz would have been initiated by subglacial outflow; it seems unlikely that this outflow would have overtopped the LIS. The closest

modern analogue to Lake Agassiz outburst floods are Icelandic *jökulhlaups* (Björnsson, 2003).

The essential physics of subglacial outburst flooding relates to the stability of a subglacial drainage conduit connecting a reservoir of stored water to a subaerial or submarine outlet some distance downstream from the reservoir. For water to flow from the reservoir to an outlet, a hydraulic gradient must exist and the conduit must not seal off. Whether a flood develops depends on the outcome of a competition between processes that enlarge the drainage conduit and processes that shrink it. Energy is dissipated by flowing water and some of this energy is transferred to the conduit walls causing ice to melt. Ice overburden pressure can differ from the water pressure in the conduit and if ice pressure exceeds water pressure then the differential pressure will lead to creep closure of the conduit. In a typical outburst flood the channel enlargement process dominates as the flood intensifies; the flood is terminated when the reservoir has drained or water pressure in the conduit decreases to the point that the creep closure process is vigorously activated and the flood terminates by sealing off the drainage path. The physics of subglacial outburst flooding has received considerable attention (e.g. Mathews, 1973; Björnsson, 1974, 1992; Nye, 1976; Spring, 1980; Spring and Hutter, 1981, 1982; Clarke, 1982; Fowler and Ng, 1996; Ng, 1998; Fowler, 1999) although only Shoemaker (1992) has applied this understanding to discussion of floods from Lake Agassiz. Recently Clarke (2003) has developed a new computational model, based on the formulation of Spring and Hutter, that we shall here apply to the problem of Lake Agassiz drainage. The governing equations of the model are summarized in Appendix A.

### 3.1. Geometrical considerations

Geometrical constraints exert an important influence on outburst flooding but are challenging to obtain. Just before Lake Agassiz drained, the ice margins that helped control its volume, as well as the proximity to the Tyrrell Sea and potential flood routings, were highly mobile. Isostatic adjustments accompanying the rapid disintegration of the Laurentide Ice Sheet introduce uncertainty concerning the relative elevation of the Lake Agassiz water plane and the Tyrrell Sea. Because of uncertainty surrounding the precise ice margins and flood routings we consider three possible configurations of the ice margins and a total of six alternative flood routings (Figs. 1–4).

#### 3.1.1. Reservoir geometry and lake levels

The maximum volume of Lake Agassiz was associated with the Kinojévis level during which Lake Agassiz (to the west) and Lake Ojibway (to the east) coalesced to form a superlake. Separate investigations of

the two lakes led to the identification of the Ponton stage of Lake Agassiz and the Kinojévis stage of Lake Ojibway (Vincent and Hardy, 1979) which are now regarded as a single stage of the superlake (Thorleifson, 1996; Leverington et al., 2002a; Teller et al., 2002). Leverington et al. (2002a) suggest that the Kinojévis level may not represent the final stage of the superlake, noting that a lower beach in the Agassiz part of the
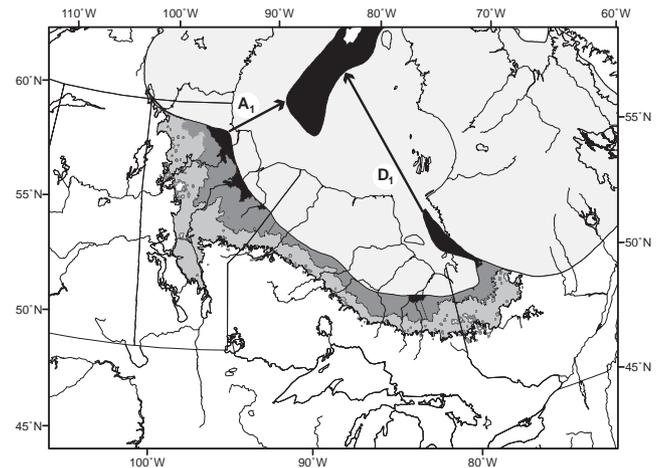


Fig. 2. Assumed ice margins and prospective drainage routings for floods occurring at 7800 $^{14}$C yr BP. Routing $A_1$ is in the vicinity of Churchill, MB and routing $D_1$ is in the vicinity of James Bay. The lake areas corresponding to the Kinojévis level (medium grey) and the Fidler level (dark grey) are shaded. The Tyrrell Sea and that part of Lake Agassiz that lies below sea level are shaded black. Note that owing to the reservoir geometry at 7800 $^{14}$C yr BP neither routing $A_1$ nor $D_1$ can drain the entire lake to sea level.
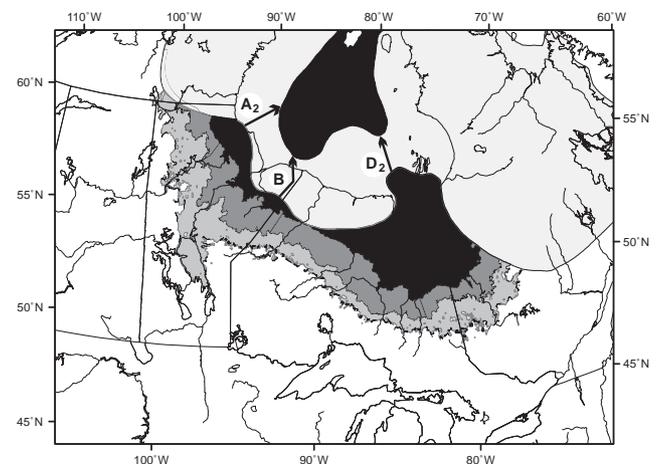


Fig. 3. Assumed ice margins and prospective drainage routings for floods occurring at 7700 $^{14}$C yr BP. Routing B is in the vicinity of the Nelson River Estuary and routing $D_2$ is in the vicinity of James Bay. Ice cover is indicated by light grey shading. The lake areas corresponding to the Kinojévis level (medium grey) and the Fidler level (dark grey) are shaded. The Tyrrell Sea and that part of Lake Agassiz that lies below sea level are shaded black. Note that according to our geometric reconstruction the entire above-sea-level volume of the lake can be drained by a flood following routing $A_2$, B or $D_2$.
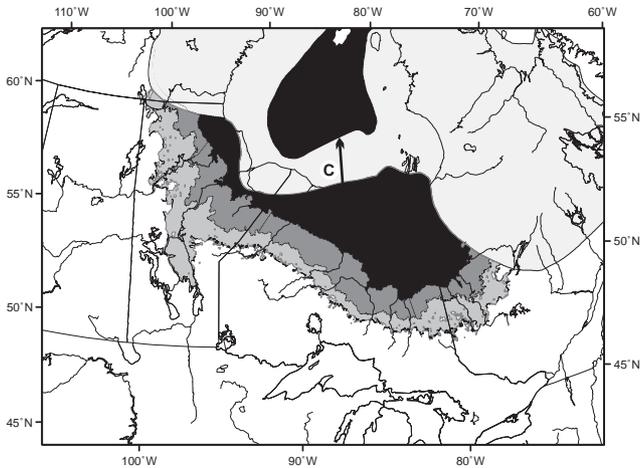
Fig. 4. Adjusted ice margins and prospective drainage routing C for a flood occurring at 7700 ^{14}C yr BP or shortly thereafter. The lake areas corresponding to the Kinojévis level (medium grey) and the Fidler level (dark grey) are shaded. The Tyrrell Sea and that part of Lake Agassiz that lies below-sea-level are shaded black. Note that according to our geometric reconstruction the entire above-sea-level volume of the lake can be drained by a flood following routing C.

basin (the Fidler beach, Klassen, 1983; Thorleifson, 1996) may represent a later level of the lake; a beach near modern Lake Abitibi in the Ojibway portion of the basin may be correlable (Veillette et al., 2003).

To calculate the reservoir geometry of the superlake, we employ the methods described by Mann et al. (1999) and Leverington et al. (2002b). Based on modern topographic data ($30 \times 30$ arcsec cells; GLOBE Task Team, 1999) and bathymetric data for Hudson Bay ($5 \times 5$ arcmin cells; National Geophysical Data Center, 1988), a digital elevation model (DEM) of the present day topographic surface was constructed. Although higher-resolution databases are available, their use is unwarranted for the area and volume calculations that are fundamental to our study. From the DEM a paleotopographic surface was generated by applying a spatially smooth isostatic adjustment derived from the isobases of Teller and Thorleifson (1983, Fig. 1), linearly extrapolated northward into the Hudson Bay region using the general isobase trends of Dyke (1996) as a guide. The database of paleotopography was projected from rectangular coordinates to the Lambert Conformal Conic projection. The procedure is identical to that used by Leverington et al. (2002a) although, in detail, our volume estimates differ slightly because we adopt more recent reconstructions of the ice margin position (Dyke et al., 2003). The lake surface elevation at the Kinojévis level is taken as 230 m above the level of the Tyrrell Sea, based on comparison between the Kinojévis level and the level at which the flood topographic model approximates the extent of post-glacial marine submergence in the southern Hudson Bay lowlands (e.g. Dredge and Cowan, 1989; Vincent, 1989).

To acknowledge uncertainty in both the ice margin positions and the timing of flood release we consider three possible configurations of the superlake. Fig. 2 is based on the Dyke et al. (2003) ice margins for 7.8 ^{14}C kyr BP (light grey shading) and shows the area of Lake Agassiz at the Kinojévis level (medium grey) as well as its area if water level dropped to the elevation of the Tyrrell Sea (black). A small fraction of the lake volume lies below sea level and could not participate in a flood. The lake area corresponding to the Fidler level, which we take as 127 m above the Tyrrell Sea, is also indicated (dark grey). Note that as lake level drops to sea level the reservoir divides into separate basins, implying that in the final stages of a flood following routing $A_1$ water in the eastern portion of the reservoir would become isolated and unavailable to sustain the flood. Likewise a flood following routing $D_1$ could not extract all the water of the western portion of the reservoir.

Fig. 3 is comparable to Fig. 2 but is based on the Dyke et al. (2003) ice margins for 7.7 ^{14}C kyr BP. The sea-level area of the lake (black) indicates that the western and eastern portions of the reservoir remained confluent, or nearly so, when water level dropped to sea level so that the entire above-sea-level lake volume is available to each of the candidate outlets. The area corresponding to the Fidler level is also indicated (dark grey). Finally, Fig. 4 presents an adjusted version of the ice margins in Fig. 3. The motivation for this adjustment is to lend plausibility to a flood following routing C, a path which lies along the "meltwater channels" identified by Josenhans and Zevenhuizen (1990) (Fig. 1), but would not be preferred if the ice margins of Fig. 3 are accepted.

The geometric description required for the flood simulation model involves the hypsometric function (area vs. elevation) for the reservoir but modified to reflect the availability of water to various flood routings (Fig. 5). As discussed, the water volumes available to routings $A_1$ and $D_1$ differ and this explains the difference between the curves labelled $A_1$ and $D_1$ in Fig. 5. The step in the two curves, at roughly 100 m a.s.l., corresponds to the elevation at which the reservoir divides into distinct western and eastern sub-reservoirs. All the above sea-level lake volume is available to routings $A_2$, B and $D_2$ so a single curve describes the hypsometry for these outlets. In Fig. 5 the graphs depict the function $Z_L(A)$ where $Z_L$ is lake level and $A$ is lake area. Interchanging the axes in Fig. 5 is equivalent to expressing the functional relationship in the form $A(Z_L)$ which is straightforwardly related to the lake volume as a function of elevation
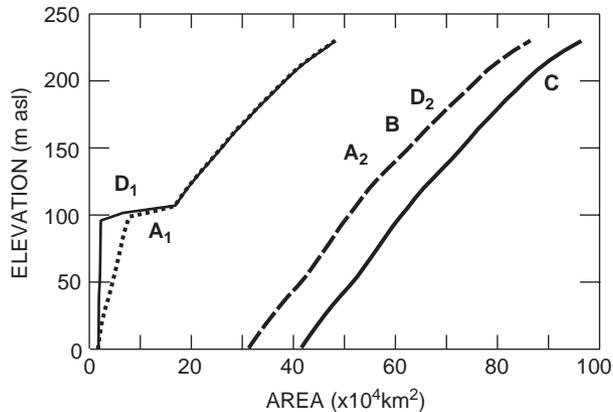
$$V(Z_L) = \int_0^{Z_L} A(z)\, dz.$$

Fig. 5. Hypsometric curves appropriate to the proposed drainage routings. These curves differ from the conventionally defined elevation vs. area curves because they are specific to individual routings and describe the water volume that is available to contribute to a flood following that path. In the case of routings $A_1$ and $D_1$ the available water volume differs from the above-sea-level lake volume. The horizontal step that appears in the curves for $A_1$ and $D_1$ coincides with the elevation at which the Lake Agassiz reservoir divides into western and eastern sub-volumes. Routings $A_2$, B and $D_2$ can capture the entire above-sea-level volume of the lake as can routing C. The area and lake volume associated with C are somewhat greater than for $A_2$, B and $D_2$.

### 3.1.2. Ice margins and drainage routings

We have already touched upon ice margins and drainage routings but only in the context of their implications for the availability and volume of water. Since publication of the paleogeographic reconstructions of Dyke and Prest (1987), speculation concerning drainage routings has been guided by their suite of maps that depict the position of the LIS margin for 13, 12, 11, 10, 9, 8.4, 8 and 7 ^{14}C kyr time slices (plus others not relevant to the lake history). The 8.4 ^{14}C kyr time slice is described as the "last time which we can say with some confidence predates breakup of the LIS by incursion of the sea into Hudson basin." Recently Dyke et al. (2003) have updated these paleogeographic reconstructions, accepting revised regional marine reservoir corrections, assimilating previous knowledge (e.g. Vincent and Hardy, 1979; Dredge, 1983; Klassen, 1983), updating this knowledge (e.g. Josenhans and Zevenhuizen, 1990), and synthesizing this information to resolve more finely the deglaciation of North America. Their time slices at 7.8, 7.7 and 7.6 ^{14}C kyr BP are especially relevant to the present study. According to these reconstructions, the complete disintegration of the ice dam between Lake Agassiz and the Tyrrell Sea occurred between 7.7 and 7.6 ^{14}C kyr BP. Thus the 7.8 and 7.7 ^{14}C kyr ice margin reconstructions represent the spatial relationships between ice and water at the time when one or more outburst floods were released. Dating uncertainty is approximately ±100 yr.

The most probable routing for a subglacial outburst is one that minimizes the distance between the tunnel entry

and exit. Such a routing leads to the maximum hydraulic head gradient and, typically, a low ice divide elevation along the flood path. Highly plausible routings are associated with the seams between the disintegrating Keewatin, Hudson and Labrador sectors of the ice sheet. The locations of these seams are marked by the presence of interlobate moraines delineating the Keewatin–Hudson convergence near Churchill, MB (Dredge, 1983; Klassen, 1983) and the Hudson–Labrador convergence near James Bay (Skinner, 1973; Hardy, 1977). The opening of these seams created embayments in the ice dam that were occupied by antecedent lakes Agassiz (west seam) and Ojibway (east seam), which eventually coalesced to form superlake Agassiz.

Among many possibilities we consider six candidate flood routings (Fig. 1 and Table 1). We do not suggest that all of these routings were used because, in some sense they are competing for the role of flood channel. If more than one outburst occurred, for example an initial flood from the Kinojévis level and a second flood from the Fidler level (Leverington et al., 2002a; Teller et al., 2002), the flood routings may have differed. Routings $A_1$ and $D_1$ are consistent with the 7800 ^{14}C BP ice margins of Dyke et al. (2003) and correspond respectively to a flood path following the Keewatin–Hudson seam ($A_1$) identified by Klassen (1983) and the Hudson–Labrador seam ($D_1$) identified by Vincent and Hardy (1979). The lengths of the two paths are 321 and 789 km, respectively. A flood following routing $A_1$ could explain the arcuate scours noted by Josenhans and Zevenhuizen (1990) although orientation of the scour axes is not well aligned with water following this routing (Fig. 1). Western routings would provide a plausible explanation for a distinctive red clay layer (Kerwin, 1996) found in early postglacial marine sediments in cores from northern Hudson Bay and western Hudson Strait. This layer is known from direct dating to be correlative with the flood event and to have been deposited rapidly over a great distance (Barber et al., 1999). The most likely source of red sediment is the red till spread widely into northwestern Hudson Bay after glacial erosion of the Dubawnt Group bedrock in Keewatin (Shilts, 1980). Farther eastward dispersion of red debris by icebergs would have occurred as a calving bay propagated toward Manitoba (Figs. 2 and 3). However, the most intensive pulse of icebergs out of this bay would reasonably have accompanied catastrophic lake drainage. In contrast, eastern drainage routes, such as $D_1$, would have intersected little if any ice carrying red debris. A small percentage of the till covering Coats Island is of Dubawnt origin and would have been exposed to the currents and iceberg transport associated with all of the proposed flood routes, including $D_1$. Thus the presence of the distinctive red clay layer cannot be uniquely associated with western routings. Although we have indicated path $D_1$ as a candidate, it is an

Table 1
Candidate drainage routings

| Outlet location | | Date BP | | Conduit entry | | Conduit exit | | Length (km) |
|---|---|---|---|---|---|---|---|---|
| | | ($^{14}$C yr) | (Cal yr) | Lat (°N) | Long (°W) | Lat (°N) | Long (°W) | |
| $A_1$ | Churchill River, MB | 7800 | 8600 | 58.75 | 95.00 | 60.00 | 89.90 | 320.6 |
| $A_2$ | Churchill River, MB | 7700 | 8450 | 59.01 | 93.93 | 59.82 | 90.63 | 207.2 |
| B | Nelson River, MB | 7700 | 8450 | 55.75 | 91.20 | 57.40 | 89.90 | 215.1 |
| C | Winisk, ON | 7700[a] | 8450 | 56.00 | 85.10 | 58.00 | 84.75 | 223.4 |
| $D_1$ | James Bay, ON/QC | 7800 | 8600 | 54.14 | 80.17 | 60.94 | 83.96 | 789.1 |
| $D_2$ | James Bay, ON/QC | 7700 | 8450 | 56.33 | 81.39 | 57.91 | 82.27 | 183.2 |

[a] Adjusted ice margin.

improbable selection owing to its length. We introduce it for discussion purposes to acknowledge that in the absence of convincing alternatives it has tended to receive favour (e.g. Barber et al., 1999, Fig. 1) although precise flood routings have not been critical to previous discussions.

Routings $A_2$, B and $D_2$ are associated with embayments of Lake Agassiz appearing in the Dyke et al. (2003) ice margin reconstruction for 7700 $^{14}$C BP and have comparable lengths of 207, 223 and 183 km, respectively. Geomorphic evidence of high water discharge lends support to either of the two western paths, with path B being preferred to path $A_2$ because it follows a large channel incised below the Tyrrell Sea marine limit (Prest et al., 1968) and because it is better aligned with the sand waves and arcuate iceberg scours (Fig. 1). The "dog-leg" associated with path B is not an essential feature but represents an attempt to acknowledge the mapped channel shape; if the path were straightened the length would decrease by around 7%, a small influence relative to other sources of uncertainty. In terms of length, $D_2$ is the most favoured but we find no persuasive offshore geomorphic support for this routing. Veillette (1994, pp. 966–967) comments that "most of the erosional features associated with the catastrophic drainage are probably masked by Tyrrell Sea sediments." Shortly before 7800 $^{14}$C yr BP a south-flowing ice stream formed in James Bay (Veillette, 1997); the associated drawdown of the ice sheet surface along the Hudson–Labrador seam could have been conducive to the establishment of subglacial drainage to the Tyrrell Sea following $D_2$.

Our motivation for proposing path C as a candidate flood routing is its proximity to meltwater channels near the contemporary outlet of Winisk River, ON (Fig. 1). This would not be a preferred routing given the Dyke et al. (2003) 7700 $^{14}$C BP ice margins so, to add plausibility to this routing, we have revised the margins and labelled the edited margins as 7.7 kyr*. The revision could be justified as rectifying a possible error in the Dyke et al. (2003) reconstruction or as representing the ice marginal position at some time shortly after 7700 $^{14}$C BP. The path length for route C is 223 km.

Following an outburst, the flood channel either remains open or reseals so that lake level rises until a subsequent flood is released. If resealing does occur this discharge is temporarily interrupted but the stored freshwater is ultimately delivered as an abrupt water pulse to Hudson Bay; any subsequently formed lake would contain new meltwater. Opening and maintaining a stable channel to Hudson Bay would not preclude a subsequent subglacial flood developing along another routing if the rapidly changing ice marginal positions and ice thickness favoured this. Thus $(A_1 \oplus D_1) + (A_2 \oplus B \oplus D_2) + C$ or $(A_1 \oplus A_2 \oplus B) + D_2$ are possible multiflood scenarios where the symbol $\oplus$ denotes the exclusive OR logical operator (XOR), e.g. $B \oplus C$ reads "either B or C but not both". Provenance data for red bed deposits in Hudson Strait (Barber, 2001) are compatible with multiple outburst pulses.

Taking into account geological evidence and other factors, our preferred path for the initial (Kinojévis level) flood is B because this is the most consonant with the location and orientation of the sand waves and arcuate iceberg scours in Hudson Bay (Fig. 1). Our preferred path for a subsequent flood (Fidler level) is path C where wide meltwater channels provide convincing geomorphic evidence for a flood, though one of lesser magnitude than that which generated the bathymetrically mapped sand waves and arcuate icebergs scours.

### 3.1.3. Bed and ice topography

Bed and ice surface topography along the candidate flood paths are required to calculate the ice overburden pressure which activates the tunnel closure process in the simulation model. Bed topography is obtained from the isostatically adjusted digital elevation model described in Section 3.1.1 and is generated by sampling the DEM at points along the proposed flood paths (Table 1 and Figs. 1–4).

Although there are few observational constraints on the ice surface topography around 7.8–7.7 $^{14}$C kyr BP, the situation is less problematic than it might seem. If the flood release is supraglacial, then the ice surface elevation along the flood route must nowhere exceed the lake surface elevation $Z_L$. If the flood release is

subglacial, a necessary condition for the development of an outburst flood is that the ice overburden pressure $p_i(s) = \rho_i g[(Z_s(s) - Z_b(s)]$ does not greatly exceed the subglacial water pressure. At the upstream endpoint $(s = 0)$ of a subglacial tunnel the water pressure is simply $p_w = \rho_w g[Z_L - Z_b(0)]$ where $Z_L$ is the lake surface elevation. At the downstream endpoint $(s = l_0)$ the water pressure is $p_w = \rho_w g[Z_{SL} - Z_b(l_0)]$ where $Z_{SL} = 0$ is the elevation of mean sea level (taken as 0 m a.s.l. in our study). Thus, assuming ice flotation at the endpoints, a simple calculation gives the endpoint ice surface elevations as

$$Z_s(0) = Z_b(0) + \frac{\rho_w}{\rho_i}[Z_L - Z_b(0)],$$

$$Z_s(l_0) = Z_b(l_0) + \frac{\rho_w}{\rho_i}[Z_{SL} - Z_b(l_0)].$$

Between the endpoints, the ice surface cannot be substantially greater than $Z_s(0)$ or the near-flotation requirement would be violated. To generate an ice surface profile, we assume a cubic form $Z_s(s) = A + Bs + Cs^2 + Ds^3$, position the ice divide at $s_d$, between $s = 0$ and $s = l_0$, and assign an elevation $Z_s(s_d)$ that gives a visually pleasing profile. If the assigned value of $Z_s(s_d)$ is too large, a flood will not develop and a lower value must be chosen. As a consequence there is very little latitude in assigning the surface geometry and very little effect on the hydrographs, assuming conditions permit a flood to develop in the first place.

Fig. 6 illustrates the bed and ice surface profiles along the six candidate flood paths. For paths $A_2$, B, C and $D_2$ we indicate both the Kinojévis and Fidler levels and plot ice surface topography appropriate for each level. Key geometrical properties for the various paths, including maximum ice thickness, are summarized in Table 2.

## 3.2. Material properties

Most of the relevant material properties of ice and water (Table 3) are well known and the small degree of uncertainty in their values contributes insignificant changes in model predictions. The deformation properties of ice are the notable exception. These are encapsulated in the parameters $B$ and $n$ of the experimentally based flow law for ice $\dot{\varepsilon} = (\sigma/B)^n$ (Glen, 1955), also expressed in the form $\dot{\varepsilon} = A\sigma^n$, where $\dot{\varepsilon}$ is shear strain rate, $B$ and $A$ are temperature-dependent coefficients, $\sigma$ is shear stress and $n$ the flow law exponent. The flow law coefficient $B$ (or $A$) is affected by ice temperature, fabric and impurity content; thus for a given glaciological setting there is substantial uncertainty in its value. For the reference models we take $n = 3$ and accept recommended values for temperate ice (Paterson, 1994), i.e. ice at its melting temperature. It is a simple matter to convert from one definition of the
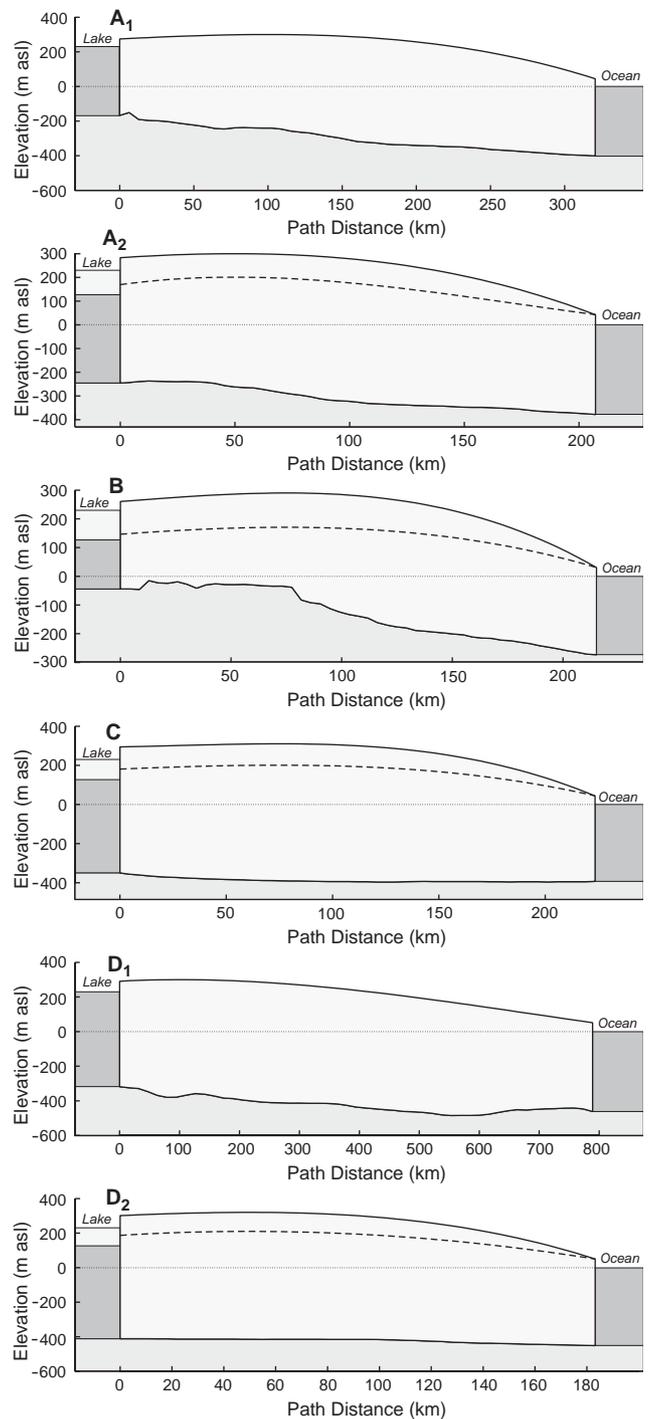


Fig. 6. Assumed flood path geometry associated with the proposed drainage routings. The routing endpoints correspond to those indicated in Figs. 1–4 and summarized in Table 1. Bed topography is obtained from a digital elevation model adjusted for isostatic tilting. The lake surface elevation when filled to its maximum (Kinojévis) level is 230 m above the elevation of the Tyrrell Sea. A possible late filling known as the Fidler stage is also indicated for routings $A_2$, B, C and $D_2$. We take this filling level to be 127 m above the level of the Tyrrell Sea. Ice surface profiles have been generated using a cubic function constrained to yield ice flotation at the upstream and downstream endpoints of the drainage path. Ice thickness at the ice crest cannot greatly exceed the ice flotation thickness or a subglacial outburst flood could not develop.

Table 2
Elevation data for reference drainage routings and filling levels

| Model | Conduit entry | | Conduit exit | | Ice crest | | Maximum | |
|---|---|---|---|---|---|---|---|---|
| | Bed (m a.s.l.) | Surface (m a.s.l.) | Bed (m a.s.l.) | Surface (m a.s.l.) | Surface | distance | Thickness | distance |
| | | | | | (m a.s.l.) | (km) | (m) | (km) |
| $A_1(230)$ | −167 | 274.1 | −401 | 44.6 | 300 | 100 | 608.2 | 178.2 |
| $A_2(230)$ | −246 | 282.9 | −378 | 42.0 | 300 | 50 | 604.7 | 92.6 |
| $A_2(127)$ | −246 | 168.4 | −378 | 42.0 | 200 | 50 | 502.2 | 92.6 |
| $B(230)$ | −44 | 260.4 | −273 | 30.3 | 290 | 75 | 444.8 | 132.2 |
| $B(127)$ | −44 | 146.0 | −273 | 30.3 | 170 | 75 | 339.3 | 134.9 |
| $C(230)$ | −350 | 294.4 | −393 | 43.7 | 310 | 75 | 701.2 | 86.2 |
| $C(127)$ | −350 | 180.0 | −393 | 43.7 | 200 | 75 | 591.4 | 86.2 |
| $D_1(230)$ | −319 | 291.0 | −462 | 51.3 | 300 | 100 | 692.8 | 239.3 |
| $D_2(230)$ | −411 | 301.2 | −451 | 50.1 | 320 | 50 | 734.9 | 52.4 |
| $D_2(127)$ | −411 | 186.8 | −451 | 50.1 | 210 | 50 | 624.9 | 52.4 |

All elevations are relative to Tyrrell Sea level (the maximum marnie limit elevation). Pre-flood lake surface is assumed to be 230 m a.s.l.

Table 3
Parameters for the reference models

| Property | Value | Units |
|---|---|---|
| *Material properties* | | |
| Density of water, $\rho_w$ | 1000 | kg m$^{-3}$ |
| Density of ice, $\rho_i$ | 900 | kg m$^{-3}$ |
| Specific heat capacity of water, $c_w$ | 4271.7 | J kg$^{-1}$ K$^{-1}$ |
| Thermal conductivity of water, $K_w$ | 0.558 | W m$^{-1}$ K$^{-1}$ |
| Latent heat of melting for ice, $L$ | $3.335 \times 10^5$ | J kg$^{-1}$ |
| Pressure melting coefficient, $c_T$ | $7.5 \times 10^{-8}$ | K Pa$^{-1}$ |
| Viscosity of water, $\mu_w$ | $1.787 \times 10^{-3}$ | Pa s |
| Flow law exponent, $n$ | 3 | |
| Flow law coefficient, $B$ | $5.28 \times 10^7$ | s$^{1/n}$ |
| | | |
| *Geophysical properties* | | |
| Gravity acceleration, $g$ | 9.80 | m s$^{-2}$ |
| Lake temperature, $T_L$ | 4 | °C |
| Manning roughness, $\langle n' \rangle$ | 0.03 | m$^{1/3}$ s |
| Input discharge to lake, $Q_L$ | 100,000 | m$^3$ s$^{-1}$ |
| | | |
| *Numerical parameters* | | |
| Number of grid points, $N$ | 51 | |
| Numerical compressibility, $\beta$ | $1.0 \times 10^{-7}$ | Pa$^{-1}$ |
| Relative tolerance for integration | $1.0 \times 10^{-4}$ | |
| Absolute tolerance for integration | $1.0 \times 10^{-7}$ | |
| Initial conduit cross-sectional area | 10 | m$^2$ |

flow law coefficient to the other using the relation $A = 1/B^n$.

## 3.3. Geophysical parameters

In addition to the geometric properties of the reservoir and drainage path and the material properties of ice and water, geophysical parameters such as lake temperature, input discharge to the reservoir and the hydraulic roughness of the drainage conduit influence the magnitude, duration and character of outburst floods. These are not well constrained by observations and therefore deserve individual discussion.

### 3.3.1. Lake temperature

Little is known about the temperature of Lake Agassiz water, although there would have been a regular supply of 0°C water from the LIS throughout its history. In the latter stages of its existence, relevant to our study, Licciardi et al. (1999) calculated that precipitation contributed about twice that of meltwater to the basin, and we feel it is reasonable to assume that this runoff into Lake Agassiz was well above 0°C during the summer. Based on analysis of ostracode assemblages in Lake Agassiz sediments in the Lake Manitoba basin, Curry (1997) concluded that the southern part of Lake Agassiz had a mean water temperature of about 5°C. A rough energy balance analysis for the lake at the Upper Campbell stage (9.4 ^{14}C kyr BP) suggested that water temperature probably did not exceed 5°C (Mann et al., 1997). Given these scant indications, we chose 4°C (the temperature at which water has maximum density) as a reference value for water temperature (Table 3).

### 3.3.2. Input discharge to reservoir

Licciardi et al. (1999) present the most recent and most authoritative attempt to quantify the deglacial runoff attending the disintegration of North American ice sheets. Appendix A of Licciardi et al. (1999) shows the discharge through the St. Lawrence drainage system decreasing from 0.1524 Sv at 8.4–7.7 ^{14}C kyr BP to 0.0609 Sv at 7.7–7.0 ^{14}C kyr BP, a reduction of 91, 500 m$^3$ s$^{-1}$. At the same time these changes are occurring in the St. Lawrence system, the runoff through Hudson Strait increases from 0.0552 to 0.1718 Sv, corresponding to an increase in discharge of 116, 600 m$^3$ s$^{-1}$. Most of this change can be attributed to redirection of inflow waters to the Lake Agassiz

reservoir. The average of the two discharge estimates is $104,050$ m³ s⁻¹ and we take this as justification of our assignment of $Q_L = 100,000$ m³ s⁻¹ in Table 3.

### 3.3.3. Hydraulic roughness

The turbulent flow of water in pipes and natural conduits such as rivers and subglacial tunnels is resisted by the frictional interaction between water and its confining boundaries. Empirically, this interaction is characterized by the Manning roughness parameter $n'$ (e.g. Dingman, 1984). A representative value for the Manning roughness of a polished metal pipe is $n' \sim 0.01$ m⁻¹ᐟ³ s and for a boulder-strewn river $n' \sim 0.1$ m⁻¹ᐟ³ s. Estimating the Manning roughness for outburst flood conduits is more challenging and our approach is to calibrate the flood simulation model by adjusting the value of Manning roughness in order to match observed hydrographs for known outburst floods from "Hazard Lake", Yukon, Canada (Clarke, 1982), Summit Lake, BC, Canada (Clarke and Mathews, 1981) and Grímsvötn, Iceland (Björnsson, 1992). From this calibration study it was found that for "Hazard Lake" $n' = 0.045$ m⁻¹ᐟ³ s; for Summit Lake $n' = 0.023$ m⁻¹ᐟ³ s and for Grímsvötn $n' = 0.032$ m⁻¹ᐟ³ s (Clarke, 2003). Based on these results we shall take $n' = 0.03$ m⁻¹ᐟ³ s as the reference value for Manning roughness.

### 3.3.4. Numerical analysis

The simulation equations were solved using MATLAB with the `ode15s` integrator. The absolute integration tolerance was set to $1.0 \times 10^{-7}$ and the relative tolerance to $1.0 \times 10^{-4}$ (the default settings are $1.0 \times 10^{-6}$ and $1.0 \times 10^{-3}$, respectively). A numerical compressibility of $\beta = 1.0 \times 10^{-7}$ Pa⁻¹ was assumed for water and this has the effect of reducing computational stiffness and accelerating the integration. By varying the error tolerances and numerical stiffness it was confirmed that varying these assignments influenced the integration time but not the computed results. The spatial grid for the reference models was chosen to have $N = 51$ grid points irrespective of the length of the flood path. As an initial condition for each flood simulation, it was assumed that a small semi-circular conduit having a cross-sectional area of 10 m² connected the entry and exit points of the subglacial tunnel. If the ice overburden pressure is too high this initial conduit will close off and no flood can occur, otherwise the initial conduit grows to release an outburst flood. For some models, e.g. the $D_1$ reference model, the time required for the initial conduit to develop into a large flood conduit can exceed 10 yr. If a smaller initial conduit were assumed, this growth phase would have even longer duration although the ultimate flood magnitude and the duration of the flood phase would be unaffected. Thus the assignment of the initial conduit cross section is largely a practical matter.

## 4. Results

To gain insight into the expected magnitude and duration of outburst floods from Lake Agassiz we consider six candidate drainage paths ($A_1$, $A_2$, B, C, $D_1$, $D_2$) and two different filling levels for the reservoir. The 230 m level corresponds to the Kinojévis stage of Lake Agassiz and the 127 m level a.s.l. to the Fidler stage. To distinguish the various possibilities we denote, for example, a Kinojévis flood following path B as B(230) and a Fidler flood following this path as B(127). We do not consider Fidler level floods following paths $A_1$ and $D_1$ because we regard these paths as candidate paths for an initial (Kinojévis) flood but imagine that a subsequent (Fidler) flood in the same region would follow the shorter paths $A_2$ or $D_2$; thus the total number of reference models is 10. In addition to our study of the reference models we also consider the sensitivity of the reference models to changes in poorly known input parameters.

### 4.1. Reference models

Simulation results for the 10 reference models are presented in Fig. 7 and Table 4. Hydrographs are time shifted with respect to each other in order to distinguish the graphs and simplify comparison among models. Thus, for example, there is no significance to the fact that the peak in the hydrograph for $A_1$ precedes that for $D_1$ by roughly 0.75 yr (Fig. 7a). Table 4 summarizes the main characteristics of each reference flood simulation. Note that we distinguish between the available water volume and the actual flood volume. The available water volume is path specific and corresponds to the water volume that could be delivered along a particular drainage path if the lake level dropped to sea level. The flood volume is the actual volume released in a given flood. The sea level equivalent for each flood is also calculated (Table 4) taking $3.62 \times 10^{14}$ m² as the ocean area (e.g. Menard and Smith, 1966). Interestingly, and somewhat to our surprise, none of the reference floods terminated by complete evacuation of the available water volume. Rather, the lake level dropped to an intermediate elevation and either stabilized at that elevation (if the flood conduit remained open) or began to rise (if the flood conduit sealed off). The calculated peak discharge for various reference floods ranged from 3.82 Sv for $A_1$(230) to 8.99 Sv for C(230) with a representative duration of $\sim 0.5$ yr. In all cases Kinojévis-level floods exceeded the magnitude of Fidler level floods following the same path. The final state of the flood conduit is noted as either "open" or "sealed" and
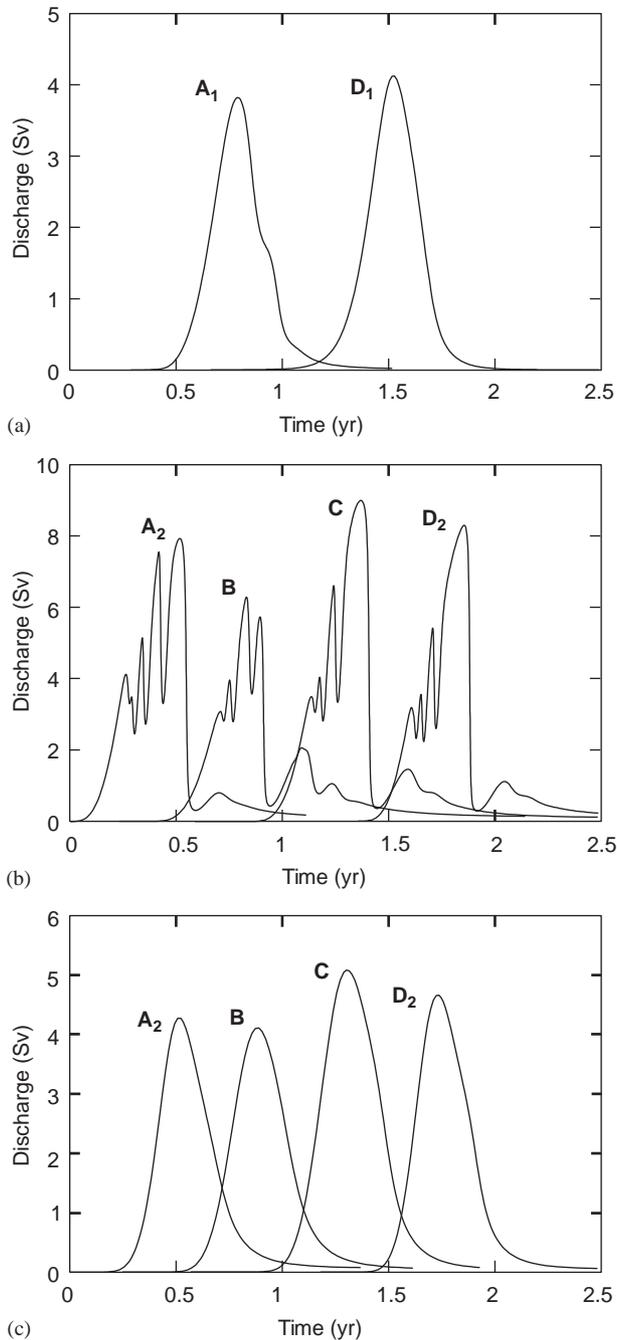
Fig. 7. Simulated discharge hydrographs for the reference models and various flood routings and filling levels. Note that to improve clarity the individual hydrographs have been time-shifted; thus relative timings have no significance. (a) Hydrographs for routings $A_1$ and $D_1$, appropriate to floods occurring ca. 7800 ^{14}C yr BP and a reservoir filled to the Kinojévis level (230 m). (b) Hydrographs for routings $A_2$, B, C and $D_2$, appropriate to floods occurring ca 7700 ^{14}C yr BP and a reservoir filled to the Kinojévis level (230 m). (c) Hydrographs for routings $A_2$, B, C and $D_2$ appropriate to floods occurring ca 7700 ^{14}C yr BP and a reservoir filled to the Fidler level (127 m).

this distinction also influences how we summarize modelling results (Table 4). For conduits that remain open, the concept of flood volume is ambiguous.

Suppose, for example, that the input flow to the reservoir is $Q_L = 100,000$ m$^3$ s$^{-1}$ as we assume for the reference models. Once the flood phase has terminated a flow of 100,000 m$^3$ s$^{-1}$ persists through the flood conduit and over time this extra water volume becomes appreciable. Clearly it is desirable to attempt a separation of the flood component of the flow from the base line component. Our method of achieving this is to define the flood volume as that part of the total flow that exceeds the input flow once the flood has developed (Fig. 8). To calculate the total water release, the flood contribution and the base flow contribution *after initiation of the flood* are added. In addition to freshwater from Lake Agassiz, Hudson Bay would also be receiving meltwater runoff from the disintegrating ice masses that bordered it (Licciardi et al., 1999).

We now comment on the results of the individual reference model simulations. The three panels of Fig. 7 group together floods for the 7.8 ^{14}C kyr BP and Kinojévis filling level, $A_1(230)$ and $D_1(230)$ (Fig. 7a); floods for the 7.7 kyr and 7.7 kyr* margins and the Kinojévis filling level, $A_2(230)$, B(230), C(230) and $D_2(230)$ (Fig. 7b); and floods for 7.7 kyr and 7.7 kyr* margins and the Fidler filling level, $A_2(127)$, B(127), C(127) and $D_2(127)$ (Fig. 7c). Despite the difference in flood routing, hydrographs for reference models $A_1(230)$ and $D_1(230)$ (Fig. 7a) show comparable magnitude and duration for the outburst. Both hydrographs indicate a peak discharge of roughly 4 Sv and a flood duration of 0.5 yr, however the two floods terminate in a different manner. For $A_1(230)$ the flood terminates with the drainage conduit remaining open and a constant outflow of $Q_L$ flowing through it; for $D_1(230)$ the flood terminates when the conduit is sealed by creep closure of the ice walls.

The hydrographs for the 7.7 kyr and 7.7 kyr* margins and Kinojévis filling level (Fig. 7b) are genuinely surprising and reveal a multipulse structure that has not been encountered in previous modelling studies, in part because simplified models cannot exhibit such complex behaviour. Although surprising, the multipulse structure of the hydrographs is unquestionably an expression of the model physics rather than a computational artifact. This suite of models ($A_2(230)$, B(230), C(230), $D_2(230)$) yields the most intense floods; the largest water release and the most intense flood are associated with model C(230). The peak discharge for C(230) is 9 Sv and the flood volume has a sea-level equivalent flood volume of 20 cm. In every case the flood terminates with a stable drainage channel open to the Tyrrell Sea.

Despite the lower lake level and reduced reservoir volume, hydrographs for the 7.7 kyr and 7.7 kyr* margins and Fidler level (Fig. 7c) produce vigorous floods with peak discharge in the range 4–5 Sv and a typical duration of 0.5 yr. Like the previous suite of

Table 4
Flood characteristics for reference models

| Model | Water volume | | | Water level | | Peak discharge (Sv) | Final state |
|---|---|---|---|---|---|---|---|
| | Available (km$^3$) | Flood | | Initial | minimum | | |
| | | (km$^3$) | (m SLE) | (m a.s.l.) | (m a.s.l.) | | |
| A$_1$(230) | 43,400 | 27,900[a] | 0.08 | 230.0 | 155.9 | 3.82 | Open |
| A$_2$(230) | 128,100 | 63,300[a] | 0.17 | 230.0 | 143.9 | 7.92 | Open |
| A$_2$(127) | 55,700 | 36,600[a] | 0.10 | 127.0 | 53.7 | 4.28 | Open |
| B(230) | 128,100 | 53,900[a] | 0.15 | 230.0 | 158.5 | 6.28 | Open |
| B(127) | 55,700 | 36,400[a] | 0.10 | 127.0 | 48.4 | 4.11 | Open |
| C(230) | 151,400 | 70,800[a] | 0.19 | 230.0 | 144.9 | 8.99 | Open |
| C(127) | 68,500 | 47,900[a] | 0.13 | 127.0 | 41.2 | 5.08 | Open |
| D$_1$(230) | 40,600 | 36,800 | 0.10 | 230.0 | 129.8 | 4.12 | Sealed |
| D$_2$(230) | 128,100 | 62,600[a] | 0.17 | 230.0 | 144.8 | 8.30 | Open |
| D$_2$(127) | 55,700 | 38,700[a] | 0.11 | 127.0 | 42.9 | 4.66 | Open |

The available volume is the volume lying above sea level which could be delivered to the Tyrrell Sea following a given path. The flood volume is the actual volume released during a flood. SLE (sea level equivalent) is calculated taking the ocean area as $3.62 \times 10^{14}$ m$^2$.

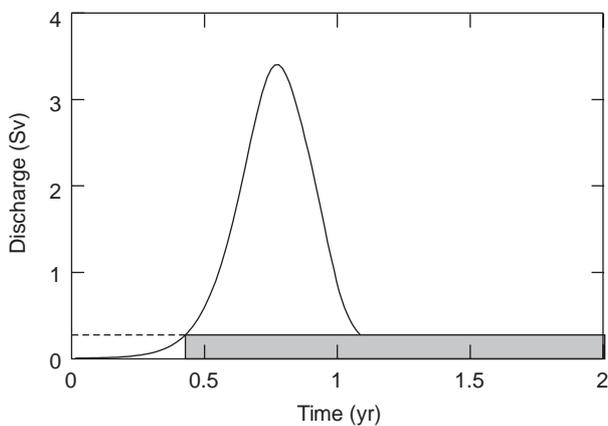[a] Excludes base flow contribution.



Fig. 8. Calculation of flood volume. For floods that terminate with the drainage path remaining unsealed we remove the base flow contribution as indicated. Note that a small pre-flood contribution from the base flow is included with the calculated flood volume. For floods that terminate by sealing the drainage path we calculate volume by simply integrating the hydrograph over the time from the initiation to the termination of the flood.

models, these floods terminate with the drainage channel open to the Tyrrell Sea but the hydrographs have simple form and lack the multipulse structure of those shown in Fig. 7b.

### 4.2. Sensitivity tests

Comparison of results for the reference models confirms a general consistency between comparable suites of hydrographs, indicating that the assignment of the drainage path and other geometric details are not sources of large variability in the model predictions. Other sources of model variability are now examined. Specifically, we explore the sensitivity of models A$_1$(230) and C(230) to changes in lake temperature, hydraulic roughness and flow law stiffness. Additionally, we use model A$_1$(230) to demonstrate that uncertainty in the input discharge $Q_L$ has a negligible influence on model predictions.

Fig. 9a shows the effect of changing lake temperature on the simulated hydrograph for model A$_1$(230). The middle curve corresponds to the reference model (4°C) and we bracket this model by comparing it to simulations for 2°C and 6°C water. Clearly water temperature is a sensitive parameter of the model with high temperature yielding a high peak discharge. This result is not surprising because enlargement of the drainage tunnel by melting is the process that allows the flood to develop. Thermal energy from the lake supplements the thermal energy released by viscous dissipation and increases the melting rate.

Fig. 9b illustrates the effect of varying the Manning roughness of the drainage conduit. The middle curve ($n' = 0.03$) corresponds to the hydrograph for the A$_1$(230) reference model and the adjacent curves correspond to smoothing ($n' = 0.03$) and roughening ($n' = 0.04$) the conduit walls. The sensitivity tests indicate that hydraulic roughness is a moderately sensitive parameter of the model and, as expected, a smooth-walled conduit yields more intense floods than a rough-walled conduit. A second interesting result of this comparison is that the previously noted multipulse character of the discharge hydrograph seems to be favoured if the conduit is smooth-walled.

Fig. 9c shows the influence of stiffening and softening the ice flow law coefficient while fixing the flow law exponent at $n = 3$. The middle curve corresponds to the hydrograph for the A$_1$(230) reference model and the adjacent curves correspond to stiffening the ice by halving the value of the flow law coefficient $A$ from $6.7936 \times 10^{-24}$ to $3.3968 \times 10^{-24}$ Pa$^{-3}$ s and softening it by doubling this coefficient from $6.7936 \times 10^{-24}$ to
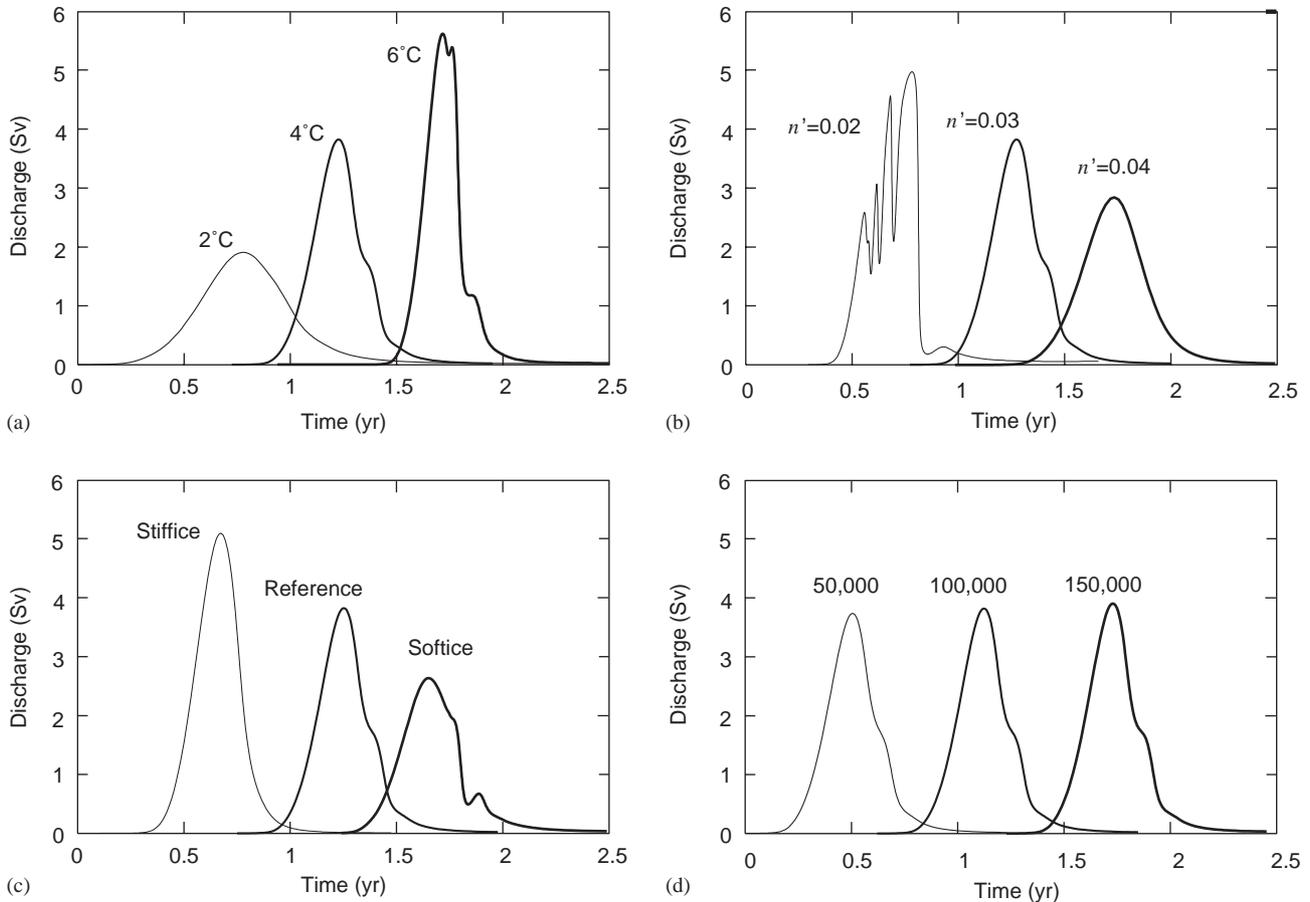
Fig. 9. Sensitivity testing of hydrographs for routing $A_1$ and Kinojévis filling level. Note that to improve clarity the individual hydrographs have been time-shifted; thus relative timings have no significance. (a) Effect of varying lake temperature. (b) Effect of varying Manning roughness of drainage conduit. (c) Effect of altering the flow law for ice. (d) Effect of varying the input discharge to the reservoir.

$13.5872 \times 10^{-24}$ Pa$^{-3}$ s. Recall that two different forms of the flow law are commonly used for glaciological calculations. Applying the conversion relationship $B = (1/A)^{1/n}$ gives the corresponding values of the alternative flow law coefficient as $B = 5.28 \times 10^7$ Pa s$^{1/n}$ (reference value), $B = 6.6524 \times 10^7$ Pa s$^{1/n}$ (stiff ice) and $B = 4.1907 \times 10^7$ Pa s$^{1/n}$ (soft ice). Clearly, varying the flow law coefficient affects the form and magnitude of the simulated hydrographs. Increased peak discharge is associated with stiff ice because the ice closure process is less effective at shrinking the drainage conduit. Note that softer ice also introduces a more complex character to the shape of the hydrograph.

Finally we demonstrate that the input discharge to the lake has a negligible effect on the form and magnitude of the simulated hydrographs for model $A_1(230)$ (Fig. 9d). The middle curve corresponds to the reference value for $Q_L$ (100,000 m$^3$ s$^{-1}$).

Repeating the sensitivity analysis for the C(230) model, we again find that increasing lake temperature increases the peak discharge (Fig. 10b). Additionally, the specific character of the multipulse hydrograph is affected by water temperature. Varying hydraulic roughness (Fig.

10b) also affects the discharge hydrographs, though in a more complicated manner. Unlike the comparable sensitivity test for $A_1(230)$ we do not find that the peak discharge is associated with the smoothest conduit. However a detailed examination of the results of this sensitivity test, including modelling intermediate values of roughness in the range $0.02 < n' < 0.03$, confirms that there is a consistent relationship between flood volume and hydraulic roughness, with the greatest water release being associated with the smoothest conduit. The test of sensitivity to changes in $B$ yields qualitative results similar to those for $A_1(230)$. For stiff ice the maximum discharge is greater than that for soft ice (Fig. 10c). As well, the multipulse structure of the hydrograph is affected by varying $B$. A test of the sensitivity of model C(127) to variations in the input discharge was also performed and, as expected, this was negligible.

## 5. Discussion

As for most physical models there is a selection of the physical processes that are considered and those that are
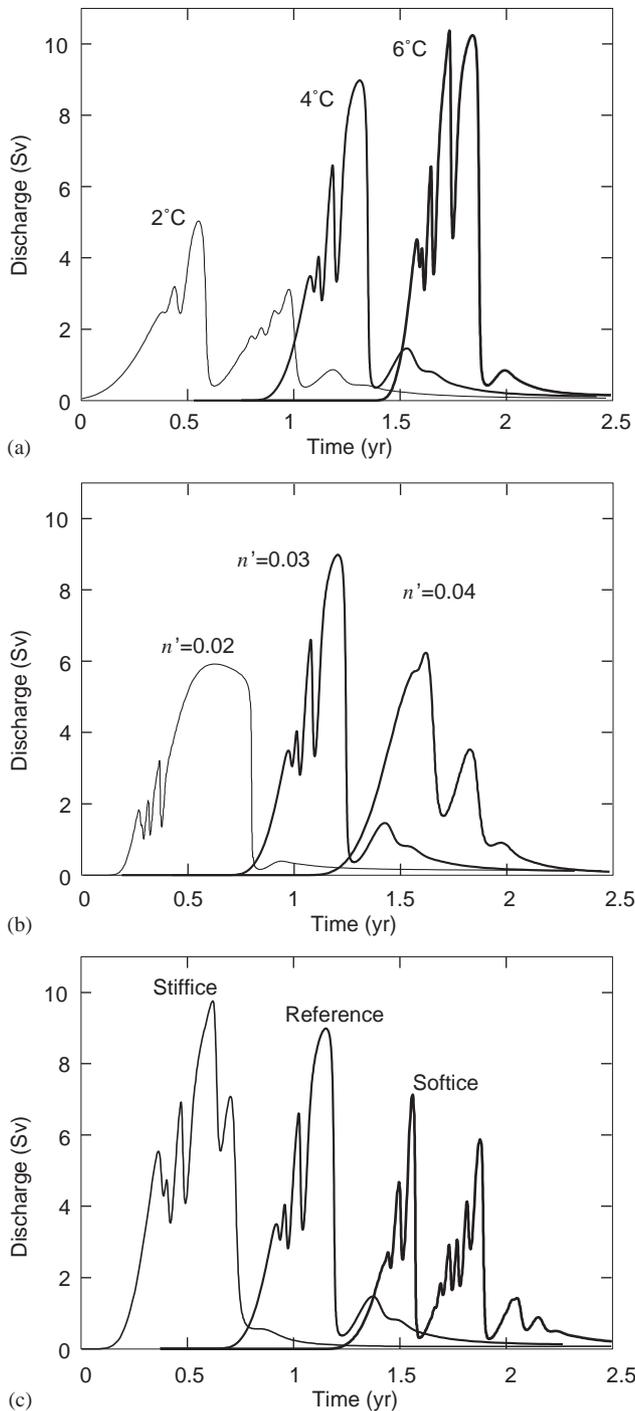
Fig. 10. Sensitivity testing of hydrographs for routing C and Kinojévis filling level. Note that to improve clarity the individual hydrographs have been time-shifted; thus relative timings have no significance. (a) Effect of varying lake temperature. (b) Effect of varying Manning roughness of drainage conduit. (c) Effect of altering the flow law for ice.

ignored. Thus the full range of natural responses cannot be faithfully represented. One of the most interesting results of our study is that multipulse hydrographs can emerge spontaneously as an expression of the model physics. We have performed modelling studies to find

the explanation of this unexpected feature of the hydrographs and have established that the multipulse character is associated with the formation of transient localized flow constrictions in the drainage conduit. Such constrictions can develop when water pressure in the conduit drops substantially below ice overburden pressure at some point along the flow path. As long as flow past the constriction can occur, the discharge $Q$ through the constriction is essentially equal to the discharge immediately upstream and downstream from it. (A small difference is possible if there is freezing or melting at the ice walls.) Because $Q = vS$, where $v$ is the cross-sectionally averaged water velocity and $S$ is the cross-sectional area of the conduit, $v$ must increase in order to compensate for a decrease in $S$. The increase in $v$ is caused by an increase in the gradient of the fluid potential $\phi = p_w + \rho_w g Z_b$ across the constricted zone. It follows that in the vicinity of a constriction the water pressure upstream from the constriction can differ substantially from the water pressure downstream from it. An increase in upstream water pressure tends to oppose the channel closure process that created the constriction and the increase in $v$ as water flows past the constriction leads to increased viscous dissipation and melting downstream from it. Together the two processes can remove constrictions before they completely seal off the flow. It is the creation and destruction of flow constrictions that produces pulse-like fluctuations in the simulated flood hydrographs.

We have examined the computational aspects of flow constrictions. For model C(230) the detailed structure of the hydrograph is unaffected by increasing or decreasing the numerical compressibility and integration accuracy parameters by an order of magnitude or by changing the MATLAB integrator from ode15s to ode23s. However the detailed structure is influenced by changing the sampling density of the spatial grid, i.e. by increasing or decreasing $N$ from its reference value of $N = 51$. This is not a desirable outcome and it expresses the fact that the model behaviour is sensitive to the length scale of the flow constrictions as well as to the overall length of the conduit. For $N = 51$ and a conduit length $l_0 = 223$ km (as for the C reference model) the spatial sampling interval is roughly 4.5 km and this is the smallest length scale which can be resolved by that model. Increasing $N$ decreases this minimum length scale but at the cost of a rapidly increasing computational burden, because decreasing the spatial sampling interval demands a compensating decrease in the integration time step. Thus the difficulty cannot be circumvented in this manner. Despite the fact that the detailed character of multipulse hydrographs is affected by the assignment of $N$, we find that the predicted flood volume remains unaffected. Comparing the predicted flood volume for model C(230) and grid sizes of $N = 11$, 21, 31, 41, 51, 61, 71, 81, 91 indicates that the flood

volume differs, at most, by 0.05% from the mean value for these runs. Thus, although the details of individual hydrographs and predicted peak discharge vary as $N$ is increased, the predicted flood volume release does not.

Uncertainty surrounds the conditions that controlled the termination of outburst floods from Lake Agassiz. In many contemporary outburst floods the channel growth process dominates until the reservoir is emptied, at which point the flood terminates. The fact that none of the simulated floods was terminated by completely draining the available water volume indicates that the creep closure was sufficiently active to prevent this outcome. Yet $D_1(230)$ was the only reference model simulation that terminated by sealing off the drainage tunnels. For the rest, the flood terminated when a stable drainage tunnel was established. The physics of stable drainage tunnels has been described in classic papers (Röthlisberger, 1972; Shreve, 1972) and glaciologists refer to these tunnels as R channels to acknowledge Röthlisberger's seminal contribution.

It would be parsimonious to attribute the Fidler stage to incomplete drainage of waters at the Kinojévis lake stage, rather than to complete drainage of the available lake water followed by a partial refilling. In reality, however, it is unlikely that a stable R channel would form under the conditions attending outburst floods from Lake Agassiz. Our assumption that the inflow to the reservoir is $Q_L = 100,000$ m$^3$ s$^{-1}$ obscures the fact that $Q_L$ would be expected to have a strong seasonal cycle so that steady conditions could not possibly prevail in the drainage channel. A second complication, reflecting a limitation of the model, is that creep closure is the only conduit closure process that is considered. Close examination of the output for the various reference models reveals that during outburst floods the conduit radius can become very large—comparable to the thickness of the ice sheet. Under such circumstances, collapse of the ice roof is a likely outcome. Depending on whether the infalling ice plugs the conduit or is efficiently evacuated, one can foresee that the flood will either terminate by the formation of an ice jam in the conduit or the latter part of the flood will exit through a subaerial canal rather than a subglacial tunnel. Thus, in reality, there is substantial uncertainty as to whether there was partial or complete emptying of the available water volume during floods from Lake Agassiz.

Our calculations of volume for the final stages of glacial Lake Agassiz–Ojibway are similar to those of Leverington et al. (2002a), who used the same isostatically adjusted model with slightly different ice margins. They calculated the total volume of freshwater at 163,000 km$^3$ (including water below the level of the Tyrrell Sea); in a two-step drawdown alternative, they calculated that the outburst drained 113,100 km$^3$ from the Kinojévis level and, shortly afterward, 49,900 km$^3$ from the Fidler level. They estimated the one-step

outburst would have taken 1 yr, generating a flux of 5.2 Sv, in contrast to their two-step flux of 3.6 and 1.6 Sv (Teller et al., 2002). In terms of the ocean response to Lake Agassiz outbursts, the most important results of the flood simulation modelling are that the flood phase was likely to have been short, probably less than 1 yr, and that the simulation modelling, which suggests that full drainage of the reservoir did not occur for any of the reference floods, is likely to be conservative in terms of the estimated flood volume. Table 4 compares flood volume to the available water volume and this percentage varies from 42% (B(230)) to 91% ($D_1(230)$).

Paleoenvironmental evidence suggests the climate signal of the 8.2 cal kyr BP event had a duration of roughly 200 yr or less and did not follow a simple pattern of deterioration and recovery but was two-pronged in character (Alley et al., 1997; von Grafenstein et al., 1998; Baldini et al., 2002). Modelling studies (Renssen et al., 2001, 2002) indicate that a simple freshwater forcing of the Labrador Sea, the release of 1.5 Sv for an interval of 10 yr or of 0.75 Sv sustained for 20 yr, can yield a complicated climate response. Such models ignore many effects from mixing and dilution of the freshwater pulse en route to the Labrador Sea. Our study suggests that the forcing itself could be complex. Multiple floods from Lake Agassiz, for example from the Kinojévis (230 m) and Fidler (127 m) levels, are a strong possibility. For multiple floods to have occurred, either the ice dam reformed on at least one occasion or the lake dropped to a level at which it temporarily stabilized before a subsequent flood, possibly following a different path, was released. The interval between a first and second flood would depend on the precise details of the situation but an interval of 10–50 yr between an initial flood and a subsequent one seems reasonable. Table 5 summarizes reservoir refilling times from sea level to the Kinojévis and Fidler levels for various routings, assuming an inflow of $Q_L = 100,000$ m$^3$ s$^{-1}$.

Multipulse floods are a second manner of introducing a complex freshwater forcing. Despite some caveats concerning our ability to simulate their detailed

Table 5
Reservoir filling times

| Outlet | Water level | | Time (yr) |
|---|---|---|---|
| | Initial (m a.s.l.) | Final (m a.s.l.) | |
| $A_1$ | 0 | 230 | 13.8 |
| $A_2$, B, $D_2$ | 0 | 230 | 40.6 |
| | 0 | 127 | 17.7 |
| C | 0 | 230 | 48.0 |
| | 0 | 127 | 21.7 |
| $D_1$ | 0 | 230 | 12.9 |

Input discharge is taken as $Q_L = 100,000$ m$^3$ s$^{-1}$.

structure, the possibility of such floods is predicted by our modelling study. As yet it is unclear how climate system models would respond to sub-annual complexity of the freshwater forcing.

## 6. Conclusions

We conclude the following:

(1) The known physics of glacier-dammed lakes strongly suggests that a terminal flood from Lake Agassiz was inevitable.
(2) The terminal flood may have occurred along any of several physically plausible routings. Pending more detailed mapping, the strongest contenders as flood paths are the Tyrrell Sea-floor channels labelled routes B and C in Fig. 1.
(3) The most probable release mechanism for the final flood from glacial Lake Agassiz was outburst flooding through a subglacial tunnel in a manner analogous to modern *jökulhlaups* from the Gríms-vötn reservoir in Iceland. Though unlikely, a supraglacial flood mechanism cannot be completely ruled out.
(4) The Fidler beach (if it is correctly interpreted as a final level of the lake) may mark the drawdown level for the Kinojévis flood rather than a refilling level.
(5) Irrespective of details of the ice margin and lake volume the outburst flood probably had a magnitude of $\sim 5$ Sv and duration of $\sim 0.5$ yr.
(6) The effect on sea level cannot have been large. The maximum effect would be associated with complete drainage of the maximum reservoir (7.7 kyr[*] ice margin and 230 m filling) to sea level. For this situation, the available flood water volume is $151,400$ km$^3$, which has a sea-level equivalent of 0.41 m but for all reference models the released volume from above sea level was considerably less than the available volume. For the maximum case (reference model C(230) in Table 4) the sea-level equivalent flood volume was 0.19 m. Even though the outburst itself does not include all freshwater in Lake Agassiz, because some lies below sea-level, all of these waters were soon integrated into the Tyrrell Sea and northern ocean system.

Our study points to the need for work on several fronts. A more detailed examination of the geomorphic record of outburst floods is warranted; it would be highly desirable to obtain geomorphically based estimates of the maximum discharge to complement the model estimates. Current theoretical models of subglacial outburst flooding make no provision for collapse of the ice roof, a likely event during huge outburst floods. This process would be extremely challenging to

model but it is important to gauge its influence. A possible approach would be to compare the predictions of subglacial and supraglacial flood models—the un-roofed subglacial tunnel being similar to a deeply excavated canal formed by a supraglacial flood. At present only a simplified model of supraglacial outburst flooding has been described in the literature (Raymond and Nolan, 2000) although Clarke (2002) has made some progress toward a more complete model.

## Appendix A. Flood model

For simplicity we assume a Cartesian coordinate system where $x$ and $y$ correspond to Easting and Northing coordinates relative to some arbitrary geographical origin and $z$ is the vertical distance above sea level. The elevation of the bed surface is $Z_b(x, y)$ and that of the ice surface is $Z_i(x, y)$. A spatially fixed subglacial drainage path is assumed to connect the entry and exit points of the conduit. Downflow distance is denoted $s$ where $s = 0$ at the entry and $s = l_0$ at the exit. The geographical coordinates of the drainage path are described by the three functions $[X_k(s), Y_k(s), Z_k(s)]$ so that an increment of path length is written

$$\mathrm{d}s = \sqrt{(\mathrm{d}x)^2 + (\mathrm{d}y)^2 + (\mathrm{d}z)^2}. \tag{A.1}$$

The equation governing water balance in the reservoir is

$$\frac{\mathrm{d}Z_L}{\mathrm{d}t} = \frac{Q_L - Q_{\mathrm{spill}} - Q(0, t)}{A(Z_L)}, \tag{A.2}$$

where $Z_L$ is the lake surface elevation, $Q_L$ is the input discharge into the lake, $Q_{\mathrm{spill}}$ is the reservoir overflow (if any) through spillways, $Q(s, t)$ is the discharge in the drainage conduit as a function of space and time and $A(Z_L)$ is the hypsometric function appropriate to the assumed flood routing.

The drainage tunnel is assumed to have semi-circular cross section with a rock floor and ice walls. The cross-sectional area $S$ can vary with time and distance along the length of the tunnel so that $S = S(s, t)$. Water pressure, velocity and temperature in the conduit are described by the functions $p_w(s, t)$, $v(s, t)$ and $T_w(s, t)$, respectively. The equations governing the evolution of the conduit and thus the progress of the outburst flood are

$$\frac{\partial p_w}{\partial t} = -\frac{1}{\beta S}\left\{\frac{\partial S}{\partial t} + \frac{\partial}{\partial s}(vS) - \frac{m}{\rho_w}\right\}, \tag{A.3}$$

$$\frac{\partial S}{\partial t} = \frac{m}{\rho_i} - 2\,\mathrm{sgn}(p_e)\left\{\frac{|p_e|}{nB}\right\}^n S, \tag{A.4}$$

$$\frac{\partial v}{\partial t} = -\frac{\partial}{\partial s}\left(\frac{1}{2}v^2 + \frac{p_w}{\rho_w} + gZ_b\right) - \frac{1}{\rho_w S}(mv + P_w\tau_0), \tag{A.5}$$

$$\frac{\partial T_w}{\partial t} = -v\frac{\partial T_w}{\partial s} + \frac{1}{\rho_w c_w S}\left\{P_w\tau_0 v\right.$$
$$\left. - m\left(L + c_w(T_w - T_i) - \frac{v^2}{2}\right)\right\}, \tag{A.6}$$

where $p_i = \rho_i g(Z_i - Z_b)$ is ice overburden pressure, $\rho_i$ is the density of ice, $p_e = p_i - p_w$ is the effective pressure, $T_i = -c_T p_w$ is the pressure melting temperature of ice, $c_T$ is the pressure melting coefficient, $Q = vS$ is the discharge in the tunnel, $f_R$ is the perimeter-averaged value of the Darcy–Weisbach hydraulic roughness parameter, $\tau_0 = \frac{1}{8}f_R\rho_w v|v|$ is the perimeter-averaged wall stress arising from turbulent flow in the conduit, $Re = 4\rho_w|v|R_H/\mu_w$ is the Reynolds number for flow in the conduit, $R_H = \pi R/[2(\pi + 2)]$ is the hydraulic radius of the semi-circular conduit, $R = \sqrt{2S/\pi}$ is the radius of the semi-circular conduit, $\mu_w$ is the viscosity of water, $Pr = \mu_w c_w/K_w$ is the Prandtl number for water, $c_w$ and $K_w$ are the specific heat capacity and thermal conductivity for water, $Nu = 0.023Re^{4/5}Pr^{2/5}$ is the Nusselt number, and $m = \pi R K_w Nu(T_w - T_i)/4LR_H$ is the ice melting rate and $L$ is the latent heat of melting for ice. Darcy–Weisbach roughness is related to the Manning roughness through the relationship

$$f_R = \frac{8gn'^2}{R_H^{1/3}}. \tag{A.7}$$

A full description of the computational model can be found in Clarke (2003).

## References

Alley, R.B., Mayewski, P.A., Sowers, T., Stuiver, M., Taylor, K.C., Clark, P.U., 1997. Holocene climatic instability: a prominent widespread event 8200 yr ago. Geology 25, 483–486.

Andrews, J.T., Maclean, B., Kerwin, M., Manley, W., Jennings, A.E., Kalls, E., 1995. Final stages in the collapse of the Laurentide Ice Sheet, Hudson Strait, Canada: [14]C AMS dates, seismic stratigraphy, and magnetic susceptibility logs. Quaternary Science Reviews 14, 983–1004.

Baldini, J.U.L., McDermott, F., Fairchild, I.J., 2002. Structure of the 8200-year cold event revealed by a speleothem trace element record. Science 296, 2203–2206.

Barber, D.C., 2001. Laurentide Ice Sheet dynamics from 35–7 ka; Sr-Nd-Pb isotopic provenance of NW North Atlantic margin sediments. PhD. thesis. Institute of Arctic and Alpine Research, University of Colorado, 160 pp.

Barber, D.C., Dyke, A., Hillaire-Marcel, C., Jennings, A.E., Andrews, J.T., Kerwin, M.W., Bilodeau, G., McNeely, R., Southon, J., Morehead, M.D., Gagnon, J.-M., 1999. Forcing of the cold event of 8,200 years ago by catastrophic drainage of Laurentide lakes. Nature 400, 344–348.

Björnsson, H., 1974. Explanation of jökulhlaups from Grímsvötn, Vatnajökull, Iceland. Jökull 24, 1–26.

Björnsson, H., 1992. Jökulhlaups in Iceland: prediction, characteristics and simulation. Annals of Glaciology 16, 95–106.

Björnsson, H., 2003. Subglacial lakes and jökulhlaups in Iceland. Global and Planetary Change 35, 255–271.

Clark, P.U., Marshall, S.J., Clarke, G.K.C., Hostetler, S.W., Licciardi, J.M., Teller, J.T., 2001. Freshwater forcing of abrupt climate change during the last glaciation. Science 293, 283–287.

Clarke, G.K.C., 1982. Glacier outburst floods from "Hazard Lake", Yukon Territory, and the problem of flood magnitude prediction. Journal of Glaciology 24, 3–21.

Clarke, G.K.C., 2002. Hydraulics of supraglacial outburst floods. American Geophysical Union Fall Meeting, San Francisco, CA, Abstracts, F303.

Clarke, G.K.C., 2003. Hydraulics of subglacial outburst floods: new insights from the Spring–Hutter formulation. Journal of Glaciology 49, 299–313.

Clarke, G.K.C., Mathews, W.H., 1981. Estimates of the magnitude of glacier outburst floods from Lake Donjek, Yukon Territory, Canada. Canadian Journal of Earth Sciences 18, 1452–1463.

Curry, B.B., 1997. Paleochemistry of lakes Agassiz and Manitoba based on ostracodes. Canadian Journal of Earth Sciences 34, 699–708.

Dingman, S.L., 1984. Fluvial Hydrology. Freeman, New York, 383pp.

Dredge, L.A., 1983. Character and development of northern Lake Agassiz and its relation to Keewatin and Hudsonian ice regimes. In: Teller, J.T., Clayton, L. (Eds.), Glacial Lake Agassiz. Geological Association of Canada Special Paper 26, pp. 117–131.

Dredge, L.A., Cowan, W.R., 1989. Lithostratigraphic record on the Ontario shield. In: Fulton, R.J. (Ed.), Quaternary Geology of Canada and Greenland. Geological Survey of Canada, Ottawa, Canada. The Geology of North America, Vol. K-1, pp. 214–235.

Dyke, A.S., 1996. Preliminary paleogeographic maps of glaciated North America. Geological Survey of Canada, Open File 3296.

Dyke, A.S., 2003. An outline of North American deglaciation with emphasis on central and northern Canada. In: Ehlers, J., Gibbard, P.L. (Eds.), Quaternary Glaciations—Extent and Chronology, Part II: North America. Elsevier Amsterdam, in press.

Dyke, A.S., Prest, V.K., 1987. Late Wisconsinan and Holocene history of the Laurentide Ice Sheet. Géographie Physique et Quaternaire 41, 237–263.

Dyke, A.S., Moore, A., Robinson, L., 2003. Deglaciation of North America. Geological Survey of Canada, Open File 1574.

Elson, J.A., 1967. Glacial Lake Agassiz. In: Mayer-Oakes, W.J. (Ed.), Life, Land and Water. University of Manitoba Press, Winnipeg, Manitoba, Canada, pp. 37–96.

Fowler, A.C., 1999. Breaking the seal at Grímsvötn. Journal of Glaciology 45, 506–516.

Fowler, A.C., Ng, F.S.L., 1996. The role of sediment transport in the mechanics of jökulhlaups. Annals of Glaciology 22, 255–259.

Glen, J.W., 1955. The creep of polycrystalline ice. Proceedings of the Royal Society of London (Series A) 228, 519–538.

GLOBE Task Team, 1999. The Global One-kilometer Base Elevation (GLOBE) Elevation Model. Version 1.0: National Oceanic and Atmospheric Administration, National Geophysical Data Center, Boulder, Colorado.

Hardy, L., 1977. La déglaciation et les épisodes lacustre et marin sur le versant québécois des basse terres de la baie de James. Géographie Physique et Quaternaire 31, 261–273.

Hass, H.C., 2002. A method to reduce the influence of ice-rafted debris on a grain size record from northern Fram Strait, Arctic Ocean. Polar Research 21, 299–306.

Hughen, K.A., Overpeck, J.T., Trumbore, S., Peterson, L.C., 1996. Rapid climate changes in the tropical Atlantic region during the last deglaciation. Nature 380, 51–54.

Jennings, A.E., Manley, W.F., MacLean, B., Andrews, J.T., 1998. Marine evidence for the last glacial advance across Eastern Hudson Strait, Eastern Canadian Arctic. Journal of Quaternary Science 13, 501–514.

Johnston, W.A., 1946. Glacial Lake Agassiz, with special reference to the mode of deformation of the beaches. Geological Survey of Canada Bulletin 7, 20pp.

Josenhans, H.W., Zevenhuizen, J., 1990. Dynamics of the Laurentide Ice Sheet in Hudson Bay, Canada. Marine Geology 92, 1–26.

Kerwin, M.W., 1996. A regional stratigraphic isochron (ca. 8000 $^{14}$C yr B.P.) from final deglaciation of Hudson Strait. Quaternary Research 46, 89–98.

Klassen, R.W., 1983. Lake Agassiz and the late glacial history of northern Manitoba. In: Teller, J.T., Clayton, L. (Eds.), Glacial Lake Agassiz. Geological Association of Canada Special Paper 26, pp. 97–115.

Klitgaard-Kristensen, D., Sejrup, H.P., Haflidason, H., Johnsen, S., Spurk, M., 1998. A regional 8200 cal. yr BP cooling event in northwest Europe, induced by final stages of the Laurentide ice-sheet deglaciation? Journal of Quaternary Science 13, 165–169.

Leverington, D.W., Mann, J.D., Teller, J.T., 2000. Changes in the bathymetry and volume of glacial Lake Agassiz between 11,000 and 9300 $^{14}$C yr BP. Quaternary Research 54, 174–181.

Leverington, D.W., Mann, J.D., Teller, J.T., 2002a. Changes in the bathymetry and volume of glacial Lake Agassiz between 9200 and 7700 $^{14}$C yr B.P. Quaternary Research 57, 244–252.

Leverington, D.W., Teller, J.T., Mann, J.D., 2002b. A GIS method for reconstruction of late Quaternary landscapes from isobase data and modern topography. Computers and Geosciences 28, 631–639.

Licciardi, J.M., Teller, J.T., Clark, P.U., 1999. Freshwater routing by the Laurentide Ice Sheet during the last deglaciation. In: Clark, P.U., Webb, R.S., Keigwin, L.D. (Eds.), Mechanisms of Global Climate Change at Millennial Time Scales. American Geophysical Union, Washington, DC, pp. 177–202.

Mann, J.D., Leverington, D., Rayburn, J.A., Grant, N., Teller, J.T., 1997. Calculating the volume and heat budget of glacial Lake Agassiz. Geological Society of America Annual Meeting. Salt Lake City, Utah. Abstracts with Program 29, A111 (Abstract 50051).

Mann, J.S., Leverington, D.W., Rayburn, J., Teller, J.T., 1999. The volume and paleobathymetry of glacial Lake Agassiz. Journal of Paleolimnology 22, 71–80.

Marshall, S.J., Clarke, G.K.C., 1999. Modeling North American freshwater runoff through the Last Glacial Cycle. Quaternary Research 52, 300–315.

Mathews, W.H., 1973. Record of two jökulhlaups. International Association of Hydrological Sciences Publication 95, 111–116.

Menard, H.W., Smith, S.M., 1966. Hypsometry of ocean basin provinces. Journal of Geophysical Research 71, 4305–4325.

National Geophysical Data Center, 1988. ETOPO 5 database: Data announcement 88-MGG-02. In: Digital Relief of the Surface of the Earth. NOAA, National Geophysical Data Center, Boulder, CO.

Ng, F.S.L., 1998. Mathematical modelling of subglacial drainage and erosion. D.Phil. Thesis, Applied Mathematics, Oxford University, 209pp.

Nye, J.F., 1976. Water flow in glaciers: jökulhlaups, tunnels and veins. Journal of Glaciology 17, 181–207.

Paterson, W.S.B., 1994. The Physics of Glaciers, 3rd Edition. Elsevier, Oxford, 480pp.

Prest, V.K., Grant, D.R., Rampton, V.N., 1968. Glacial map of Canada. Geological Survey of Canada, Map 1257A, scale 1:5 000 000.

Raymond, C.F., Nolan, M., 2000. Drainage of a glacial lake through an ice spillway. International Association of Hydrological Sciences Publication 264, 199–207.

Renssen, H., Goose, H., Fichefet, T., Campin, J.-M., 2001. The 8.2 kyr BP event simulated by a global atmosphere–sea-ice–ocean model. Geophysical Research Letters 28, 1567–1570.

Renssen, H., Goosse, H., Fichefet, T., 2002. Modeling the effect of freshwater pulses on the early Holocene climate: the influence of high-frequency climate variability. Paleoceanography 17, 10-1–10-18.

Röthlisberger, H., 1972. Water pressure in intra- and subglacial channels. Journal of Glaciology 11, 177–203.

Shilts, W.W., 1980. Flow patterns in the central North American ice sheet. Nature 286, 213–218.

Shoemaker, E.M., 1992. Water sheet outburst floods from the Laurentide Ice Sheet. Canadian Journal of Earth Sciences 29, 1250–1264.

Shreve, R.L., 1972. Movement of water in glaciers. Journal of Glaciology 11, 205–214.

Skinner, R.G., 1973. Quaternary geology of the Moose River basin, Ontario. Geological Survey of Canada Bulletin 225, 77pp.

Spring, U., 1980. Intraglazialer Wasserabfluss: Theorie und Mod-ellrechnungen. Mitteilungen der Versuchsanstalt für Hydrologie und Glaziologie Nr. 48.

Spring, U., Hutter, K., 1981. Numerical studies of jökulhlaups. Cold Regions Science and Technology 4, 227–244.

Spring, U., Hutter, K., 1982. Conduit flow of a fluid through its solid phase and its application to intraglacial channel flow. International Journal of Engineering Science 20, 327–363.

Teller, J.T., 1987. Proglacial lakes and the southern margin of the Laurentide Ice Sheet. In: Ruddiman, W.F., Wright Jr., H.E. (Eds.), North America and Adjacent Oceans during the Last Deglaciation, Vol. K-3, Geological Society of America, Geology of North America, Boulder, CO, pp. 39–69.

Teller, J.T., 1990a. Volume and routing of late glacial runoff from the southern Laurentide Ice Sheet. Quaternary Research 34, 12–23.

Teller, J.T., 1990b. Meltwater and precipitation runoff to the North Atlantic, Arctic, and Gulf of Mexico from the Laurentide Ice Sheet and adjacent regions during the Younger Dryas. Paleoceanography 5, 897–905.

Teller, J.T., 2001. Formation of large beaches in an area of rapid differential isostatic rebound: the three-outlet control of Lake Agassiz. Quaternary Sciences Reviews 20, 1649–1659.

Teller, J.T., 2003. Controls, history, outbursts, and impact of large late-Quaternary proglacial lakes in North America. In: Gillespie, A., Porter, S., Atwater, B. (Eds.), Quaternary Period in the United States, INQUA Anniversary Volume. Elsevier, Amsterdam.

Teller, J.T., Thorleifson, L.H., 1983. The Lake Agassiz–Lake Superior connection. In: Teller, J.T., Clayton, L. (Eds.), Glacial Lake Agassiz. Geological Association of Canada Special Paper 26, pp. 261–290.

Teller, J.T., Leverington, D.W., Mann, J.D., 2002. Freshwater outbursts to the oceans from glacial Lake Agassiz and their role in climate change during the last deglaciation. Quaternary Science Reviews 21, 879–887.

Thorleifson, L.H., 1996. Review of Lake Agassiz history. In: Teller, J.T., Thorleifson, L.H., Matile, G., Brisbin, W.C. (Eds.), Sedimentology, Geomorphology, and History of the Central Lake Agassiz Basin. Geological Association of Canada Field Trip Guidebook B2, pp. 55–84.

Upham, W., 1895. The glacial Lake Agassiz. US Geological Survey Monograph, Vol. 25, 658pp.

Veillette, J.J., 1994. Evolution and paleohydrology of glacial lakes Barlow and Ojibway. Quaternary Science Reviews 13, 945–971.

Veillette, J.J., 1997. Le rôle d'un courant de glace tardif dans la déglaciation de la baie James. Géographie Physique et Quaternaire 51, 141–161.

Veillette, J.J., Paradis, S.J., Thibaudeau, P., 2003. Les cartes de formations en surface de l'Abitibi, Québec. Geological Survey of Canada, Open File 1523.

Vincent, J.-S., 1989. Quaternary geology of the southeastern Canadian shield. In: Fulton, R.J. (Ed.), Quaternary Geology of Canada and Greenland, Vol. K-1, Geological Survey of Canada, Ottawa, Canada. The Geology of North America, pp. 249–275.

Vincent, J.-S., Hardy, L., 1977. L'évolution et l'extension des lacs glaciares Barlow et Ojibway en territoire québécois. Géographie Physique et Quaternaire 31, 357–372.

Vincent, J.-S., Hardy, L., 1979. The evolution of glacial Lakes Barlow and Ojibway. Quebec and Ontario. Geological Survey of Canada Bulletin 316, 18pp.

von Grafenstein, U., Erlenkeuser, H., Müller, J., Jouzel, J., Johnsen, S., 1998. The cold event 8200 years ago documented in oxygen isotope records of precipitation in Europe and Greenland. Climate Dynamics 14, 73–81.